Eur. Phys. J. E (2012) **35**: 89
DOI 10.1140/epje/i2012-12089-6

THE EUROPEAN PHYSICAL JOURNAL E

Regular Article

Active chiral fluids

S. Fürthauer[1,2], M. Strempel[1,2], S.W. Grill[1,2,a], and F. Jülicher[1,b]

[1] Max Planck Institute for the Physics of Complex Systems, Nöthnitzer Straße 38, 01187 Dresden, Germany
[2] Max Planck Institute of Molecular Cell Biology and Genetics, Pfotenhauerstraße 108, 01307 Dresden, Germany

Received 15 March 2012 and Received in final form 25 July 2012
Published online: 25 September 2012

Abstract. Active processes in biological systems often exhibit chiral asymmetries. Examples are the chirality of cytoskeletal filaments which interact with motor proteins, the chirality of the beat of cilia and flagella as well as the helical trajectories of many biological microswimmers. Here, we derive constitutive material equations for active fluids which account for the effects of active chiral processes. We identify active contributions to the antisymmetric part of the stress as well as active angular momentum fluxes. We discuss four types of elementary chiral motors and their effects on a surrounding fluid. We show that large-scale chiral flows can result from the collective behavior of such motors even in cases where isolated motors do not create a hydrodynamic far field.

1 Introduction

Biological matter is driven far from thermodynamic equilibrium by active processes on the molecular scale. These processes are usually driven by the chemical reaction of a fuel and generate spontaneous movements and mechanical stresses in the system. The prototype example are motor molecules which play a key role for dynamic processes in the cytoskeleton [1, 2]. Motors on the molecular scale are involved in many important cellular processes, such as cell locomotion [3], cell division [4–7], the beating of cilia [8, 9] and the swimming of microorganism [1, 10, 11]. Biological materials driven by molecular motors often exhibit fluid-like behaviors on long time scales and are thus called active fluids [12, 13]. On large length scales, active fluids can exhibit spontaneous flow patterns [14–16], active material stresses [17] and unconventional material properties. Many examples of active fluids are found in biology, such as the cellular actomyosin cytoskeleton [18, 19], suspensions of microswimmers [11, 20, 21] or tissues [13, 22] but artificial examples such as granular systems on a vibrating surface [23–25] have also been studied.

Most biomolecules and the structures they form are chiral. In particular, this includes force-generating processes on the molecular and cellular scale which have been studied both experimentally [8, 11, 26] and theoretically [9, 27–30]. As a consequence, microswimmers typically move on chiral trajectories [11, 31] and cilia can exhibit helical beats [9, 32, 33]. In vertebrates, the chiral beat of cilia generates fluid flows that participate in left-right symmetry breaking, an essential step in the development of the whole organism [34–36]. Because chiral processes are ubiquitous in biological systems, a complete description of active fluids should include the effects of chirality [37–39].

Recently, several approaches have been developed to describe the physical properties of active fluids both on mesoscopic [40, 41] and macroscopic scales [42–44]. The generic features of active fluids are found in the hydrodynamic limit at large length and time scales. In this limit, the dynamics of active fluids can be obtained systematically using non-equilibrium thermodynamics [45], relying only on conservation laws, broken symmetries and local thermodynamic equilibrium. Such theories take into account local polar or nematic order, which allows for the existence of anisotropic active stresses. The corresponding hydrodynamic equations are a generalization of liquid crystal hydrodynamics [46–49] to active systems. While there exists a broad understanding of the main properties of active fluids and gels, studies of the effects of chiral asymmetries of active processes are lacking.

In this paper, we present a generic description of active fluids that takes into account active chiral processes. Active force generation induces force dipoles in the material. If all forces are internal, the total force and torque vanish as required by the conservation of momentum and angular momentum. The density of force dipoles is an active stress in the material [13, 14, 17]. In addition, active chiral processes allow for the existence of active torque dipoles, which enter the conservation of angular momentum.

We start our analysis in sect. 2 by discussing the conservation of momentum and angular momentum for chiral systems. We identify four different types of elementary chiral motors that are generated by distributions of active

[a] e-mail: swgrill@gmail.com
[b] e-mail: julicher@pks.mpg.de

torque and force dipoles in the fluid. In sect. 3, we present the general theory of active chiral fluids. We keep the spin angular momentum density as a separate hydrodynamic variable generalizing previous work on passive liquid crystals [49] to active systems. We identify conjugate pairs of thermodynamic variables and write general constitutive material relations. A simplified model is discussed in sect. 4, where active antisymmetric stresses and active angular momentum fluxes are considered. Using this model, we discuss two examples: A) the hydrodynamic flow fields generated by isolated elementary motors and B) the force an active chiral fluid exerts on two plates between which it is confined. We conclude the paper with a discussion in sect. 5.

2 Active chiral fluids

We express the force and the torque balance in fluids by conservation laws for momentum and angular momentum. Based on simple symmetry arguments, we show that active angular momentum fluxes and antisymmetric stresses exist in active chiral fluids.

2.1 Antisymmetric stress and angular momentum flux

Consider a fluid described by many small-volume elements in the continuum limit. The mass density is denoted by ρ and the velocity of the centers of mass of individual volume elements by $\mathbf{v}$. The momentum density $\mathbf{g} = \rho\mathbf{v}$ obeys the conservation law

$$\partial_t g_\alpha = \partial_\beta \sigma^{\rm tot}_{\alpha\beta} + \phi^{\rm ext}_\alpha. \tag{1}$$

The total stress $\sigma^{\rm tot}_{\alpha\beta}$ is the momentum flux and the force density $\boldsymbol{\phi}^{\rm ext}$ describes externally applied forces. Greek indices denote the three spatial coordinates x, y, z. Einstein's summation convention over repeated indices is implied. The total stress can be split into three parts

$$\sigma^{\rm tot}_{\alpha\beta} = \tilde{\sigma}^{\rm tot}_{\alpha\beta} + \sigma^{{\rm tot},a}_{\alpha\beta} - P\delta_{\alpha\beta}. \tag{2}$$

Here, the isotropic pressure is $P = -(1/3)\sigma^{\rm tot}_{\gamma\gamma}$, $\tilde{\sigma}^{\rm tot}_{\alpha\beta} = (1/2)(\sigma^{\rm tot}_{\alpha\beta} + \sigma^{\rm tot}_{\beta\alpha}) + P\delta_{\alpha\beta}$ denotes the symmetric traceless part of the total stress and $\sigma^{{\rm tot},a}_{\alpha\beta} = (1/2)(\sigma^{\rm tot}_{\alpha\beta} - \sigma^{\rm tot}_{\beta\alpha})$ is the antisymmetric part of the total stress.

In the frame of reference characterized by the position vector $\mathbf{r}$, the total angular momentum density $l^{\rm tot}_{\alpha\beta}$ is conserved,

$$\partial_t l^{\rm tot}_{\alpha\beta} = \partial_\gamma M^{\rm tot}_{\alpha\beta\gamma} + \tau^{\rm ext}_{\alpha\beta} + r_\alpha \phi^{\rm ext}_\beta - r_\beta \phi^{\rm ext}_\alpha. \tag{3}$$

Here, $M^{\rm tot}_{\alpha\beta\gamma}$ denotes the total flux of angular momentum and $\tau^{\rm ext}_{\alpha\beta}$ is the externally applied bulk torque. The total angular momentum density $l^{\rm tot}_{\alpha\beta}$ consists of an orbital contribution $r_\alpha g_\beta - r_\beta g_\alpha$ due to the center-of-mass motion of individual volume elements and a spin contribution $l_{\alpha\beta} = l^{\rm tot}_{\alpha\beta} - (r_\alpha g_\beta - r_\beta g_\alpha)$, which describes the angular momentum in the rest frame of local volume elements. The spin angular momentum can thus be written as $l_{\alpha\beta} = I_{\alpha\beta\gamma\delta}\Omega_{\gamma\delta}$, where $I_{\alpha\beta\gamma\delta}$ is the moment of inertia density and $\Omega_{\gamma\delta}$ is an intrinsic rotation rate of local volume elements. Note that the antisymmetric tensors $\Omega_{\alpha\beta}$ and $l_{\alpha\beta}$ can be equivalently represented by axial vectors, $\Omega_\alpha = \epsilon_{\alpha\beta\gamma}\Omega_{\beta\gamma}/2$ and $l_\alpha = \epsilon_{\alpha\beta\gamma} l_{\beta\gamma}/2$, where $l_\alpha = I_{\alpha\beta}\Omega_\beta$ with $I_{\alpha\beta} = \epsilon_{\alpha\delta\gamma}\epsilon_{\beta\mu\nu} I_{\delta\gamma\mu\nu}$. In the following, we will use both notations interchangeably for convenience. The total flux of angular momentum can be written as

$$M^{\rm tot}_{\alpha\beta\gamma} = M^{\pi}_{\alpha\beta\gamma} + M^{\sigma}_{\alpha\beta\gamma}, \tag{4}$$

where $M^{\pi}_{\alpha\beta\gamma}$ and $M^{\sigma}_{\alpha\beta\gamma} = r_\alpha \sigma^{\rm tot}_{\beta\gamma} - r_\beta \sigma^{\rm tot}_{\alpha\gamma}$ are the fluxes of spin and orbital angular momentum, respectively. Note that $l^{\rm tot}_{\alpha\beta}$ and its flux $M^{\rm tot}_{\alpha\beta\gamma}$ are explicitely coordinate system dependent, whereas the spin angular momentum density $l_{\alpha\beta}$ and its flux $M^{\pi}_{\alpha\beta\gamma}$ do not depend on the choice of the origin of the coordinate system. Using eqs. (1) and (3), we express the balance equations for the spin and the orbital angular momentum densities

$$\partial_t (r_\alpha g_\beta - r_\beta g_\alpha) - \partial_\gamma M^{\sigma}_{\alpha\beta\gamma} = 2\sigma^{{\rm tot},a}_{\alpha\beta} + r_\alpha \phi^{\rm ext}_\beta - r_\beta \phi^{\rm ext}_\alpha, \tag{5}$$

$$\partial_t l_{\alpha\beta} - \partial_\gamma M^{\pi}_{\alpha\beta\gamma} = -2\sigma^{{\rm tot},a}_{\alpha\beta} + \tau^{\rm ext}_{\alpha\beta}, \tag{6}$$

which reveal that the antisymmetric stress $\sigma^{{\rm tot},a}_{\alpha\beta}$ describes the rate of conversion of spin to orbital angular momentum [45].

Note that it is always possible to symmetrize the stress tensor by performing a variable transformation introducing a different velocity variable [46], see appendix D. Here, we choose to keep the antisymmetric stress for clarity and conceptual simplicity.

2.2 Force and torque dipoles with chiral asymmetry

In active chiral fluids, both the antisymmetric stress $\sigma^{{\rm tot},a}_{\alpha\beta}$ and the spin angular momentum flux $M^{\pi}_{\alpha\beta\gamma}$ in general have active contributions that correspond to the existence of force and torque dipoles, which typically have a chiral asymmetry and are generated by active processes on microscopic scales. Biological examples for active processes generating torque dipoles are chiral microswimmers, such as *E. coli* [11,31] or *Volvox* [50], and the rotation of filaments induced by the action of molecular motors [26]. Note that in the absence of external forces and torques, no force and torque monopoles can exist due to momentum and angular momentum conservation. The existence of these active dipoles leads to novel material properties with chiral asymmetry.

We first consider a torque dipole consisting of two torque monopoles with torque $q_{\alpha\beta}$ separated by a distance a in a direction given by a unit vector $\mathbf{d}$, where $q_{\alpha\beta} = q\epsilon_{\alpha\beta\nu} t_\nu$ denotes a point torque that acts along the unit pseudo-vector $\mathbf{t}$ with strength q. The torque dipole located at position $\mathbf{r}_0$ generates a torque density

$$\tau_{\alpha\beta} = q_{\alpha\beta}\left(\delta\left(\mathbf{r} - \mathbf{r}_0 + \frac{a}{2}\mathbf{d}\right) - \delta\left(\mathbf{r} - \mathbf{r}_0 - \frac{a}{2}\mathbf{d}\right)\right) \tag{7}$$

$$\simeq aq\epsilon_{\alpha\beta\nu} t_\nu d_\gamma \partial_\gamma \delta(\mathbf{r} - \mathbf{r}_0), \tag{8}$$

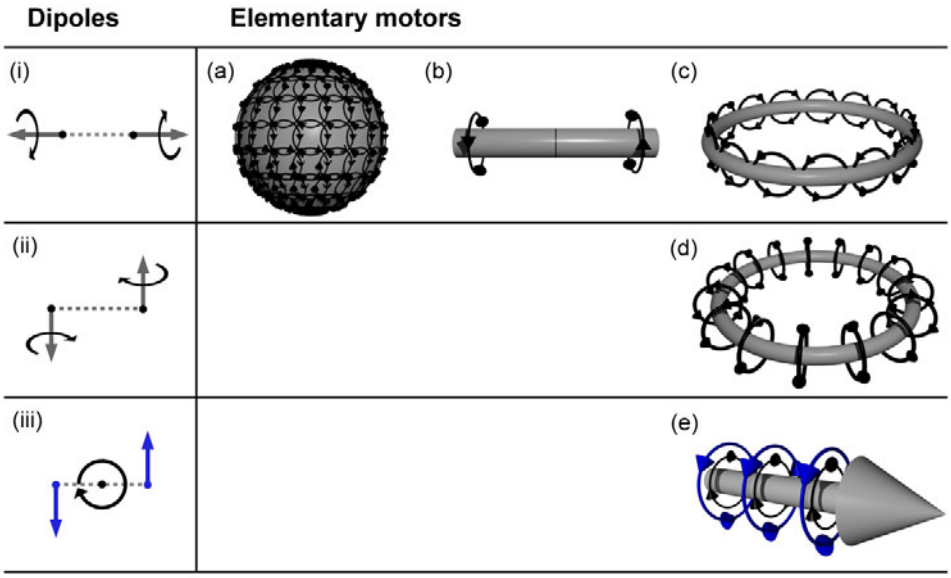

Fig. 1. Schematic representation of chiral torque and force dipoles as well as elementary motors. We distinguish two types of torque dipoles, (i) and (ii), and introduce a chiral force dipole paired with torque monopole to balance torques (iii). Here gray arrows indicate torques. Their sense of rotation is indicated by curved black arrows. Forces are indicated by blue arrows. The dipoles (i)-(iii) can be used to create the elementary motors (a)-(e) of higher symmetry. For details see text.

where eq. (8) describes the limit $a \to 0$ with qa constant. From eq. (6) we see that this active torque density $\tau_{\alpha\beta}(\mathbf{r}) = \partial_\gamma M^{\pi,\mathrm{act}}_{\alpha\beta\gamma}$ corresponds to a localized flux of angular momentum $M^{\pi,\mathrm{act}}_{\alpha\beta\gamma}(\mathbf{r}) = aq_{\alpha\beta}d_\gamma\delta(\mathbf{r}-\mathbf{r}_0)$ along the axis defined by $\mathbf{d}$.

We distinguish two different types of torque dipoles: (i) $\mathbf{t}$ parallel to $\mathbf{d}$, *i.e.* $\mathbf{t}\cdot\mathbf{d} = 1$, and (ii) $\mathbf{t}$ perpendicular to $\mathbf{d}$, *i.e.* $\mathbf{t}\cdot\mathbf{d} = 0$ (see fig. 1(i), (ii)). A general torque dipole can be expressed as a superposition of torque dipoles of type (i) and (ii). A suspension of N dipoles of type (i) with positions $\mathbf{r}^{(k)}$ and orientations $\mathbf{d}^{(k)}$, where $k = 1,\ldots,N$, generates an angular momentum flux

$$M^{\pi,\mathrm{act}}_{\alpha\beta\gamma} = qa\sum_{k=1}^{N}\epsilon_{\alpha\beta\delta}d^{(k)}_\delta d^{(k)}_\gamma\delta(\mathbf{r}-\mathbf{r}^{(k)}). \tag{9}$$

Averaging over ensembles of torque dipoles with different symmetries, we distinguish three cases: a) If the orientations of the torque dipoles are randomly distributed, the averaged active angular momentum flux becomes isotropic $M^{\pi,\mathrm{act}}_{\alpha\beta\gamma} \sim \epsilon_{\alpha\beta\gamma}$; b) in the special case that torque dipoles are exactly aligned along a unit vector $\mathbf{p}$, the angular momentum flux has the form $M^{\pi,\mathrm{act}}_{\alpha\beta\gamma} \sim \epsilon_{\alpha\beta\delta}p_\delta p_\gamma$; c) finally, if the orientations $\mathbf{d}^{(k)}$ are orthogonal to the unit vector $\mathbf{p}$ and randomly distributed in the plane perpendicular to $\mathbf{p}$, we have $M^{\pi,\mathrm{act}}_{\alpha\beta\gamma} \sim \epsilon_{\alpha\gamma\delta}p_\delta p_\beta - \epsilon_{\beta\gamma\delta}p_\delta p_\alpha$. In general, a distribution of torque dipoles of type (i) with a single axis of anisotropy defined by the vector $\mathbf{p}$ generates an angular momentum flux which is a superposition of these three cases.

These three cases differ by their symmetry. We introduce three elementary motors that locally generate the momentum fluxes with the symmetries of case (a), (b) and (c), respectively. The isotropic chiral motor corresponds to case a) and creates the local angular momentum flux $M^{\pi,\mathrm{act}}_{\alpha\beta\gamma} = \epsilon_{\alpha\beta\gamma}\delta(\mathbf{r}-\mathbf{r}_0)$, see fig. 1(a). Similarly, the chiral rod motor and chiral ring motor with $M^{\pi,\mathrm{act}}_{\alpha\beta\gamma} = \epsilon_{\alpha\beta\delta}p_\delta p_\gamma\delta(\mathbf{r}-\mathbf{r}_0)$ and $M^{\pi,\mathrm{act}}_{\alpha\beta\gamma} = (\epsilon_{\alpha\gamma\delta}p_\delta p_\beta - \epsilon_{\beta\gamma\delta}p_\delta p_\alpha)\delta(\mathbf{r}-\mathbf{r}_0)$ correspond to cases (b) and (c), see fig. 1(b), (c). Note that the angular momentum fluxes of both, the chiral rod and the chiral ring motor, are invariant under the transformation $\mathbf{p} \to -\mathbf{p}$. They therefore have a nematic symmetry.

Dipoles of type (ii) can be discussed using the same arguments. We again focus on the case where all dipoles are aligned with respect to a single axis of anisotropy $\mathbf{p}$. A new case (d) is generated by torque dipoles of type (ii) if we consider the ensemble where $\mathbf{p} = \mathbf{t}^{(k)} \times \mathbf{d}^{(k)}$ for all dipoles. In this case, $M^{\pi,\mathrm{act}}_{\alpha\beta\gamma} \sim \delta_{\alpha\gamma}p_\beta - \delta_{\beta\gamma}p_\alpha$. Note that this angular momentum flux, although generated by chiral objects, is not chiral. The elementary motor which corresponds to case (d) is the polar ring motor with $M^{\pi,\mathrm{act}}_{\alpha\beta\gamma} = (\delta_{\alpha\gamma}p_\beta - \delta_{\beta\gamma}p_\alpha)\delta(\mathbf{r}-\mathbf{r}_0)$, see fig. 1(d).

Finally, active chiral processes can also involve chiral force dipoles. A force dipole consists of two opposing force monopoles separated by a distance a in direction $\mathbf{d}$,

$$\phi_\alpha = f_\alpha\left(\delta\left(\mathbf{r}-\mathbf{r}_0+\frac{a}{2}\mathbf{d}\right)-\delta\left(\mathbf{r}-\mathbf{r}_0-\frac{a}{2}\mathbf{d}\right)\right) \tag{10}$$

$$\simeq f_\alpha a d_\beta\partial_\beta\delta(\mathbf{r}-\mathbf{r}_0). \tag{11}$$

The force dipole generates an active stress with antisymmetric part $\sigma^{a,\mathrm{act}}_{\alpha\beta} = a(f_\alpha d_\beta - f_\beta d_\alpha)\delta(\mathbf{r}-\mathbf{r}_0)/2$. Angular momentum conservation implies that this force dipole

is combined with a torque monopole $q_{\alpha\beta} = a(f_\alpha d_\beta - f_\beta d_\alpha)\delta(\mathbf{r}-\mathbf{r}_0)$, which we call dipole type (iii), see fig. 1(iii). Averaging ensembles of such force dipoles combined with torque monopoles generates active antisymmetric stresses in the system. We consider case (e) where $\mathbf{p} \sim \mathbf{d}^{(k)} \times \mathbf{f}^{(k)}$ for all k. The resulting antisymmetric stress has the form $\sigma^{a,\mathrm{act}}_{\alpha\beta} \sim \epsilon_{\alpha\beta\delta}p_\delta$. The corresponding elementary motor is the polar chiral motor with $\sigma^{a,\mathrm{act}}_{\alpha\beta} = \epsilon_{\alpha\beta\delta}p_\delta\delta(\mathbf{r}-\mathbf{r}_0)$, see fig. 1(e). In the next section, we show that the four elementary motors (a)-(c) and (e) exactly correspond to the possible terms generated by active chiral processes of different symmetry in a polar chiral fluid.

3 Generic theory of active chiral fluids

We discuss the generic theory of active chiral fluids using general principles of irreversible thermodynamics of liquid crystals [45–47]. We focus on isothermal systems and ignore heat transport. From a general expression of the local rate of entropy production, we identify conjugate pairs of thermodynamic fluxes and forces. Closely following the logic outlined in refs. [43,44] to describe active processes, we obtain constitutive material equations and dynamic equations for the active chiral fluid. In order to account for all effects relevant to active chiral processes, we keep the spin angular momentum density $\mathbf{l}$ explicitly as a slow variable [49].

3.1 Slow variables

Conservation laws and broken continuous symmetries give rise to slow, or hydrodynamic, variables. Relevant slow variables discussed here are the momentum density $\mathbf{g}$ and the spin angular momentum density $\mathbf{l}$. Because of mass conservation,

$$\partial_t\rho + \partial_\alpha(\rho v_\alpha) = 0, \tag{12}$$

the mass density ρ is also a slow variable. Here, we discuss a single component fluid with $\rho = mn$, where m is a molecular mass and n the number density. The full description of a multi-component fluid is given in appendix B. The hydrodynamic variables $\mathbf{g}$, $\mathbf{l}$ and n are completed by the polarization field $\mathbf{p}$, which characterizes the macroscopic anisotropy of the fluid. In a suspension of active swimmers, $\mathbf{p}$ describes the direction of swimmers averaged in a small volume element. In the case of the cytoskeleton, it corresponds to the local average orientation of cytoskeletal filaments. In the following, we choose $|\mathbf{p}| = 1$ since only the direction of $\mathbf{p}$ is a slow variable.

3.2 Free energy and hydrostatic properties

We consider a fluid that is divided in small volume elements, which are individually in equilibrium but not with each other. Therefore, the system globally evolves in time. Local equilibrium implies the existence of a well-defined free energy of volume elements. In the continuum limit, the free-energy density is given by

$$f(g_\alpha, l_\alpha, p_\alpha, \partial_\beta p_\alpha, n) = \frac{g_\gamma g_\gamma}{2\rho} + \frac{I^{-1}_{\gamma\delta}}{2}l_\gamma l_\delta + f_0(p_\alpha, \partial_\beta p_\alpha, n). \tag{13}$$

The first two terms of eq. (13) denote the translational and the rotational kinetic energy density and f_0 is the free energy density in the local rest frame. We introduce the chemical potential $\mu^{\mathrm{tot}} = \partial f/\partial n$ and the polar distortion field $\mathbf{h}^{\mathrm{tot}} = -\delta F/\delta\mathbf{p}$, where $F = \int_V \mathrm{d}^3x f$ is the total free energy of a volume V of fluid. Note that μ^{tot} and $\mathbf{h}^{\mathrm{tot}}$ are different from the equilibrium chemical potential $\mu = \partial f_0/\partial n$ and the equilibrium distortion field $\mathbf{h} = -\delta F_0/\delta\mathbf{p}$ by kinetic energy contributions. Here, $F_0 = \int_V \mathrm{d}^3x f_0$. The hydrostatic stress is given by

$$\sigma^e_{\alpha\beta} = (f - n\mu^{\mathrm{tot}} - g_\gamma v_\gamma - l_\gamma\Omega_\gamma)\delta_{\alpha\beta} - \frac{\partial f}{\partial(\partial_\beta p_\gamma)}\partial_\alpha p_\gamma. \tag{14}$$

It is the generalization of the hydrostatic pressure to anisotropic fluids and is known as the Ericksen stress, see appendix A. The Gibbs-Duhem relation of the system is

$$\partial_\beta\sigma^e_{\alpha\beta} = -g_\gamma\partial_\alpha v_\gamma - l_\gamma\partial_\alpha\Omega_\gamma - h^{\mathrm{tot}}_\gamma\partial_\alpha p_\gamma - n\partial_\alpha\mu^{\mathrm{tot}} \tag{15}$$

and links gradients of the hydrostatic stress to gradients of the other intensive variables of the fluid. In general, the Ericksen stress has an antisymmetric part,

$$\sigma^{e,a}_{\alpha\beta} = \frac{1}{2}\partial_\gamma M^e_{\alpha\beta\gamma} + \frac{1}{2}(h^{\mathrm{tot}}_\alpha p_\beta - h^{\mathrm{tot}}_\beta p_\alpha) - \frac{1}{2}(\Omega_\alpha l_\beta - \Omega_\beta l_\alpha), \tag{16}$$

where $M^e_{\alpha\beta\gamma} = \frac{\partial f}{\partial(\partial_\gamma p_\beta)}p_\alpha - \frac{\partial f}{\partial(\partial_\gamma p_\alpha)}p_\beta$ is the equilibrium angular momentum flux related to the polarity field.

3.3 Entropy production and constitutive relations

In an isothermal system, the total entropy production rate $\dot\Theta$ can be expressed as

$$T\dot\Theta = -\dot F + \dot W - J^{(F)}, \tag{17}$$

where dots denote time-derivatives, $W = \int \mathrm{d}V(\tau^{\mathrm{ext}}_{\alpha\beta}\Omega_{\alpha\beta}/2 + v_\alpha\phi^{\mathrm{ext}}_\alpha)$ is the work exerted on the system and $J^{(F)}$ denotes the outflux of free energy at the boundaries. Following the steps outlined in appendix B, we find

$$T\dot\Theta = \int \mathrm{d}x^3\Big\{\sigma_{\alpha\beta}u_{\alpha\beta} + \sigma^a_{\alpha\beta}(\Omega_{\alpha\beta} - \omega_{\alpha\beta}) + \frac{1}{2}M_{\alpha\beta\gamma}\partial_\gamma\Omega_{\alpha\beta} + h^{\mathrm{tot}}_\alpha\frac{D}{Dt}p_\alpha + r\Delta\mu\Big\}. \tag{18}$$

The fluid is driven out of equilibrium by the consumption of a chemical fuel at a rate r. The chemical energy difference between the fuel and its reaction products is denoted $\Delta\mu$. Here, we assume local coupling to a reservoir of fuel and reaction products such that $\Delta\mu$ is a constant. The

entropy production associated with fuel consumption is $r\Delta\mu/T$. A more general case is discussed in appendix B.

From eq. (18) we identify the following thermodynamic fluxes: the deviatoric shear stress,

$$\sigma_{\alpha\beta} = \sigma^{\rm tot}_{\alpha\beta} - \sigma^{e}_{\alpha\beta} - \sigma^{a}_{\alpha\beta} + g_\alpha v_\beta, \tag{19}$$

the deviatoric antisymmetric stress,

$$\sigma^{a}_{\alpha\beta} = \sigma^{{\rm tot},a}_{\alpha\beta} - \sigma^{e,a}_{\alpha\beta}, \tag{20}$$

the deviatoric angular momentum flux,

$$M_{\alpha\beta\gamma} = M^{\pi}_{\alpha\beta\gamma} - M^{e}_{\alpha\beta\gamma} + v_\gamma l_{\alpha\beta}, \tag{21}$$

the co-rotational time derivative of $\mathbf{p}$,

$$\frac{D}{Dt}p_\alpha = \frac{\rm d}{{\rm d}t}p_\alpha + \Omega_{\alpha\beta}p_\beta, \tag{22}$$

with the total time derivative $({\rm d}/{\rm d}t)p_\alpha = \partial_t p_\alpha + \partial_\beta(v_\beta p_\alpha)$ of $\mathbf{p}$, and the rate of fuel consumption r.

The conjugate thermodynamic forces are, respectively, the symmetric strain rate tensor $u_{\alpha\beta} = (1/2)(\partial_\alpha v_\beta + \partial_\beta v_\alpha)$, the rotational strain rate $\Omega_{\alpha\beta} - \omega_{\alpha\beta}$, the gradient of the intrinsic rotation rate $\partial_\gamma \Omega_{\alpha\beta}/2$, the polar distortion field $\mathbf{h}^{\rm tot}$ and the free-energy difference between fuel molecules and their reaction products $\Delta\mu$. Here, $\omega_{\alpha\beta} = (1/2)(\partial_\alpha v_\beta - \partial_\beta v_\alpha)$ is the vorticity.

We obtain constitutive equations by expanding the thermodynamic fluxes as linear functions of the thermodynamic forces respecting the symmetries of the system and Onsagers reciprocity principle. Here, we include all terms allowed by symmetry up to second order $\mathbf{p}$. Because of chiral asymmetry, the tensor $\epsilon_{\alpha\beta\gamma}$ can be used to create couplings that change sign under inversions of the coordinate system, *i.e.* $\mathbf{r} \to -\mathbf{r}$. For simplicity, we ignore anisotropic viscous terms and passive chiral terms, which are not the focus of this work. The constitutive equations then read

$$\begin{aligned}\sigma_{\alpha\beta} = {} & 2\eta u_{\alpha\beta} + \frac{\nu_1}{2}\left(p_\alpha h^{\rm tot}_\beta + p_\beta h^{\rm tot}_\alpha\right) + \bar\nu p_\gamma h^{\rm tot}_\gamma \delta_{\alpha\beta} \\ & + \bar\zeta \delta_{\alpha\beta}\Delta\mu + \zeta p_\alpha p_\beta \Delta\mu,\end{aligned} \tag{23}$$

$$\begin{aligned}\sigma^{a}_{\alpha\beta} = {} & 2\eta'\left(\Omega_{\alpha\beta} - \omega_{\alpha\beta}\right) + \frac{\nu_2}{2}\left(h^{\rm tot}_\alpha p_\beta - h^{\rm tot}_\beta p_\alpha\right) \\ & + \tilde\zeta \Delta\mu \epsilon_{\alpha\beta\gamma} p_\gamma,\end{aligned} \tag{24}$$

$$\begin{aligned}M_{\alpha\beta\gamma} = {} & \kappa_0 \partial_\gamma \Omega_{\alpha\beta} + \zeta_1 \epsilon_{\alpha\beta\gamma}\Delta\mu + \zeta_2 \Delta\mu \epsilon_{\alpha\beta\delta} p_\delta p_\gamma \\ & + \zeta_3 \Delta\mu(\epsilon_{\alpha\gamma\delta} p_\delta p_\beta - \epsilon_{\beta\gamma\delta} p_\delta p_\alpha) \\ & + \zeta_4 \Delta\mu(\delta_{\alpha\gamma} p_\beta - \delta_{\beta\gamma} p_\alpha),\end{aligned} \tag{25}$$

$$\begin{aligned}\frac{Dp_\alpha}{Dt} = {} & \frac{1}{\gamma} h^{\rm tot}_\alpha + \lambda_1 p_\alpha \Delta\mu - \nu_1 p_\beta u_{\alpha\beta} - \bar\nu u_{\beta\beta} p_\alpha \\ & - \nu_2\left(\Omega_{\alpha\beta} - \omega_{\alpha\beta}\right) p_\beta,\end{aligned} \tag{26}$$

$$\begin{aligned}r = {} & \Lambda\Delta\mu + \lambda_1 p_\alpha h^{\rm tot}_\alpha + \bar\zeta u_{\alpha\alpha} + \zeta p_\alpha p_\beta u_{\alpha\beta} \\ & + \tilde\zeta\left(\Omega_{\alpha\beta} - \omega_{\alpha\beta}\right)\epsilon_{\alpha\beta\gamma} p_\gamma + \frac{\zeta_1}{2}\epsilon_{\alpha\beta\gamma}\partial_\gamma \Omega_{\alpha\beta} \\ & + \frac{\zeta_2}{2}\epsilon_{\alpha\beta\delta} p_\delta p_\gamma \partial_\gamma \Omega_{\alpha\beta} + \frac{\zeta_3}{2}(\epsilon_{\alpha\gamma\delta} p_\delta p_\beta - \epsilon_{\beta\gamma\delta} p_\delta p_\alpha) \\ & \times \partial_\gamma \Omega_{\alpha\beta} + \frac{\zeta_4}{2}(\delta_{\alpha\gamma} p_\beta - \delta_{\beta\gamma} p_\alpha)\partial_\gamma \Omega_{\alpha\beta}.\end{aligned} \tag{27}$$

We have introduced the viscosities η, η' and γ. The coefficients ν_1, $\bar\nu$, and ν_2 describe the coupling between the polarity vector and velocity gradients. The coeffient κ_0 accounts for dissipative angular momentum fluxes generated by gradients of local rotation rates $\Omega_{\alpha\beta}$. The coefficient λ_1 describes magnitude changes of the vector $\mathbf{p}$ due to active processes.

The coefficient $\bar\zeta$ describes the isotropic active stresses, ζ the anisotropic active stress and $\tilde\zeta$ the active antisymmetric stress. Active antisymmetric stresses and active angular momentum fluxes appear as a result of the action of chiral motors. These contributions are represented by the coefficients ζ_1, ζ_2, ζ_3 and $\tilde\zeta$ which describe the strength and densities of isotropic, nematic rod, nematic ring and polar chiral motors, respectively, see fig. 1(a)-(c),(e). The coefficient ζ_4 describes the strengths of polar ring motors, see fig. 1(d).

Combining the conservation laws with the constitutive equations, we obtain the dynamic equations for the system. Momentum conservation implies

$$\partial_t g_\alpha = \partial_\beta\left(\sigma_{\alpha\beta} + \sigma^{a}_{\alpha\beta} + \sigma^{e}_{\alpha\beta} - g_\alpha v_\beta\right) + \phi^{\rm ext}_\alpha. \tag{28}$$

Angular momentum conservation leads to

$$\begin{aligned}\partial_t l_{\alpha\beta} = {} & \partial_\gamma\left(M_{\alpha\beta\gamma} - v_\gamma l_{\alpha\beta}\right) - 2\sigma^{a}_{\alpha\beta} - (h_\alpha p_\beta - h_\beta p_\alpha) \\ & + (\Omega_\alpha l_\beta - \Omega_\beta l_\alpha) + \tau^{\rm ext}_{\alpha\beta}.\end{aligned} \tag{29}$$

These equations are complemented by mass conservation eq. (12) and eq. (26) for the polarity dynamics. In the limit of a Newtonian fluid, we recover the Navier-Stokes equation with higher-order correction terms describing the effects of rotational strain, see appendix C.

4 Simple chiral fluids

The basic features of active chiral fluids can be highlighted by a simple case of an incompressible gel with $\partial_\alpha v_\alpha = 0$ in which we only consider the active chiral stress and active angular momentum fluxes. In particular, we ignore all passive cross-couplings for simplicity. The constitutive equations then read

$$\sigma_{\alpha\beta} = 2\eta u_{\alpha\beta}, \tag{30}$$

$$\sigma^{a}_{\alpha\beta} = 2\eta'\left(\Omega_{\alpha\beta} - \omega_{\alpha\beta}\right) + \tilde\zeta \Delta\mu \epsilon_{\alpha\beta\gamma} p_\gamma, \tag{31}$$

$$\begin{aligned}M_{\alpha\beta\gamma} = {} & \kappa_0 \partial_\gamma \Omega_{\alpha\beta} + \zeta_1 \epsilon_{\alpha\beta\gamma}\Delta\mu + \zeta_2 \Delta\mu \epsilon_{\alpha\beta\delta} p_\delta p_\gamma \\ & + \zeta_3 \Delta\mu(\epsilon_{\alpha\gamma\delta} p_\delta p_\beta - \epsilon_{\beta\gamma\delta} p_\delta p_\alpha) \\ & + \zeta_4 \Delta\mu(\delta_{\alpha\gamma} p_\beta - \delta_{\beta\gamma} p_\beta).\end{aligned} \tag{32}$$

In the low Reynolds number limit, where inertial terms are neglected, the dynamic equations are

$$\partial_\alpha \bar P = (\eta + \eta')\partial^2_\gamma v_\alpha + 2\eta'\partial_\beta \Omega_{\alpha\beta} + \partial_\beta(\tilde\zeta \Delta\mu \epsilon_{\alpha\beta\gamma} p_\gamma), \tag{33}$$

$$\begin{aligned}0 = {} & \kappa_0 \partial^2_\gamma \Omega_{\alpha\beta} + \partial_\gamma(\zeta_1 \epsilon_{\alpha\beta\gamma}\Delta\mu) + \partial_\gamma(\zeta_2 \epsilon_{\alpha\beta\delta} p_\delta p_\gamma \Delta\mu) \\ & + \partial_\gamma\left(\zeta_3 \Delta\mu(\epsilon_{\alpha\gamma\delta} p_\delta p_\beta - \epsilon_{\beta\gamma\delta} p_\delta p_\alpha)\right) \\ & + \partial_\gamma\left(\zeta_4 \Delta\mu(\delta_{\alpha\gamma} p_\beta - \delta_{\beta\gamma} p_\alpha)\right) - 4\eta'(\Omega_{\alpha\beta} - \omega_{\alpha\beta}) \\ & - 2\tilde\zeta \epsilon_{\alpha\beta\gamma} p_\gamma \Delta\mu.\end{aligned} \tag{34}$$

Here, the hydrostatic pressure $\bar{P}$ plays the role of a Lagrange multiplier. Taking the divergence of eq. (33), we find $\partial_\gamma^2 \bar{P} = 0$. Therefore, the pressure $\bar{P} = $ const if no external pressure gradients are applied. From eqs. (33) and (34) we obtain a differential equation for the flow field

$$\begin{aligned} 2\eta\partial_\gamma^2 v_\alpha = &-\partial_\beta\partial_\gamma\left\{(\zeta_2+\zeta_3)\epsilon_{\alpha\beta\delta}p_\delta p_\gamma \Delta\mu\right\} \\ &-\partial_\alpha\partial_\beta(\zeta_4\Delta\mu p_\beta) + \partial_\gamma^2(\zeta_4\Delta\mu p_\alpha) \\ &+\frac{\kappa_0}{2\eta'}\left((\eta+\eta')\partial_\gamma^4 v_\alpha + \partial_\delta^2\partial_\beta(\tilde{\zeta}\epsilon_{\alpha\beta\gamma}p_\gamma\Delta\mu)\right). \end{aligned} \tag{35}$$

4.1 Elementary motors

The active terms in eqs. (31) and (32) result from active processes that generate force and torque dipoles in the system. Following the arguments of sect. 2.2 these active contributions to the antisymmetric stress and the angular momentum flux can be interpreted as the contributions stemming from elementary motors in the material. To characterize individual elementary motors we introduce a localized activity $\Delta\mu = \Delta\mu_0\delta(\mathbf{r})$ in an otherwise passive fluid. For each active term, this local activity creates the characteristic pattern of momentum and angular momentum flux of the corresponding elementary motor, see sect. 2.2. In particular, the elementary chiral motors shown in fig. 1(a)-(c),(e) are described by the coefficients $\tilde{\zeta}$ and ζ_1, ζ_2 and ζ_3, while the coefficient ζ_4 describes the polar ring motor shown in fig. 1(d). In the following we describe the velocity fields $\mathbf{v}$ and the intrinsic rotation fields $\Omega_{\alpha\beta}$ generated by these elementary motors as solutions of eqs. (33) and (34) with the boundary conditions that $\Omega_{\alpha\beta}$ and $\mathbf{v}$ vanish at infinity.

4.1.1 Isotropic chiral motor

The isotropic chiral motor (fig. 1(a)) is described by ζ_1, with $\tilde{\zeta} = \zeta_2 = \zeta_3 = \zeta_4 = 0$. Because ζ_1 does not enter in eq. (35), the velocity field vanishes everywhere, $v_\alpha = 0$. From eq. (34) we find that the intrinsic rotation rate obeys an inhomogeneous Helmholtz equation

$$\Omega_{\alpha\beta} - \frac{\kappa_0}{4\eta'}\partial_\gamma^2\Omega_{\alpha\beta} = \frac{\zeta_1\Delta\mu_0}{4\eta'}\epsilon_{\alpha\beta\gamma}\partial_\gamma\delta(\mathbf{r}). \tag{36}$$

In spherical coordinates, the intrinsic rotation field $\Omega_{\alpha\beta}$ is thus given by $\Omega_{r\theta} = \Omega_{r\phi} = 0$ and

$$\Omega_{\theta\phi} = -\frac{\zeta_1\Delta\mu_0}{4\pi\kappa_0}e^{-2|\mathbf{r}|/\ell}\left(\frac{2}{|\mathbf{r}|\ell} + \frac{1}{|\mathbf{r}|^2}\right), \tag{37}$$

which decays on the length $\ell = (\kappa_0/\eta')^{1/2}$. Note that in the near field, for $r \ll \ell$, the intrinsic rotation rate $\Omega_{\alpha\beta}$ is different from the vorticity $\omega_{\alpha\beta}$ of the flow and that it vanishes for $\ell \ll r$.

4.1.2 Polar chiral motor

The polar chiral motor (fig. 1(d)) is described by $\tilde{\zeta}$ and $\zeta_1 = \zeta_2 = \zeta_3 = \zeta_4 = 0$. In this case the flow field does not vanish. Integrating eq. (35) yields

$$v_\alpha - \frac{\kappa_0}{4\Phi}\partial_\gamma^2 v_\alpha = \frac{\tilde{\zeta}\Delta\mu_0}{2\eta}\epsilon_{\alpha\beta\gamma}p_\gamma\partial_\beta\delta(\mathbf{r}), \tag{38}$$

where $\Phi = \eta\eta'/(\eta+\eta')$ is the harmonic mean of the viscosity and the rotational viscosity. For the velocity field $\mathbf{v}$ we find

$$v_\alpha = -\frac{\tilde{\zeta}\Delta\mu_0}{2\pi\eta}\frac{\Phi}{\kappa_0}\left(\frac{1}{r^3} + \frac{\Phi}{\kappa_0}\frac{1}{r^2}\right)e^{-|r|/\ell}\epsilon_{\alpha\beta\gamma}p_\gamma r_\beta. \tag{39}$$

The polar motor also generates an intrinsic rotation field,

$$\begin{aligned} \Omega_{\alpha\beta} = &\frac{\tilde{\zeta}\Delta\mu_0}{2\pi\kappa_0|\mathbf{r}|}\epsilon_{\alpha\beta\gamma}p_\gamma e^{-2|\mathbf{r}|/\ell} \\ &-\frac{4}{\ell^2}\int e^{-2|\mathbf{r}-\mathbf{r}'|/\ell}\frac{\omega_{\alpha\beta}}{|\mathbf{r}-\mathbf{r}'|}\mathrm{d}^3r'. \end{aligned} \tag{40}$$

The velocity field $\mathbf{v}$ and the intrinsic rotation rate $\Omega_{\alpha\beta}$ both decay on the length scale ℓ, see eqs. (38) and (40). Therefore, the polar chiral motor has no far field. Note that $\Omega_{\alpha\beta} = \omega_{\alpha\beta} = 0$ for $r \gg \ell$. Interestingly, $\Omega_{\alpha\beta} \neq \omega_{\alpha\beta}$ in the near field for $r \ll \ell$, *i.e.* the rate of intrinsic rotations differs from the vorticity of the flow.

4.1.3 Nematic chiral motors

Two nematic chiral motors exist (fig. 1(b), (c)). The chiral rod motor corresponds to $\zeta_2 \neq 0$ and $\zeta_3 = 0$ while the chiral ring motor corresponds to $\zeta_3 \neq 0$ and $\zeta_2 = 0$ with $\tilde{\zeta} = \zeta_1 = \zeta_4 = 0$. The velocity fields of these two motors are identical because ζ_2 and ζ_3 enter eq. (35) by the same term. The velocity field can be determined numerically by solving eqs. (33) and (34) using a periodic box and spatial Fourier transformations and is displayed in fig. 2(a), (b). Both nematic chiral motors induce a velocity field consisting of two opposing vortices in front and behind the motor. At the position $\mathbf{r} = 0$ the velocity field vanishes, implying that the motors do not move. The far field can be written analytically and is given by

$$v_\alpha \simeq \frac{(\zeta_2+\zeta_3)\Delta\mu_0}{4\pi\eta}\frac{\mathbf{p}\cdot\mathbf{r}}{|\mathbf{r}|^5}\epsilon_{\alpha\beta\gamma}r_\beta p_\gamma \tag{41}$$

for $r \gg \ell$. This is the same as the far field of two counter-rotating spheres separated along the vector $\mathbf{p}$ by a small distance.

The chiral rod motor and the chiral ring motor generate different intrinsic rotation fields $\Omega_{\alpha\beta}$ since ζ_2 and ζ_3 enter eq. (34) by different terms. The far field of $\Omega_{\alpha\beta}$ is given by $\Omega_{\alpha\beta} = \omega_{\alpha\beta}$, where $\omega_{\alpha\beta}$ is the vorticity of the velocity field given by eq. (41). Figure 2(c,d) and (e,f) display $\Omega_{\alpha\beta} - \omega_{\alpha\beta}$ for the chiral rod motor and the chiral ring motor. This difference is finite only in the near field.

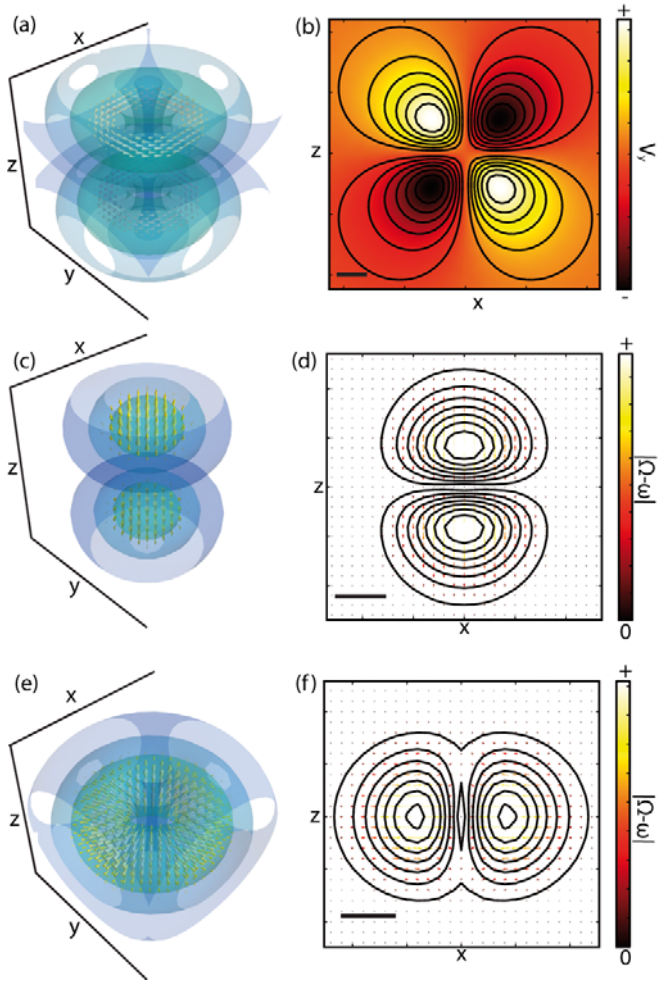

Fig. 2. Flow $\mathbf{v}$ and rotation field $\boldsymbol{\Omega} - \boldsymbol{\omega}$ of the nematic elementary motors (fig. 1(b) and (c)). Both elementary motors share the same velocity $\mathbf{v}$ shown in (a) and (b). Velocity vectors as well as surfaces of constant $|\mathbf{v}|$ are indicated in (a). The flow in the (x, z)-plane for $y = 0$ is shown in (b). The rotation fields differ for both elementary motors. The rotation field of the chiral rod is shown in (c) and (d). The rotation field of the chiral ring is shown in (e) and (f). The rotation vectors $\boldsymbol{\Omega} - \boldsymbol{\omega}$ are indicated as cones and surfaces of constant magnitude are indicated in (c) and (e). Cross-sections in the (x, z)-plane at $y = 0$ are shown in (d) and (f). The black scale bar indicates the length ℓ. The parameters are $\eta/\eta' = 1$. The size of the periodic box is 26ℓ.

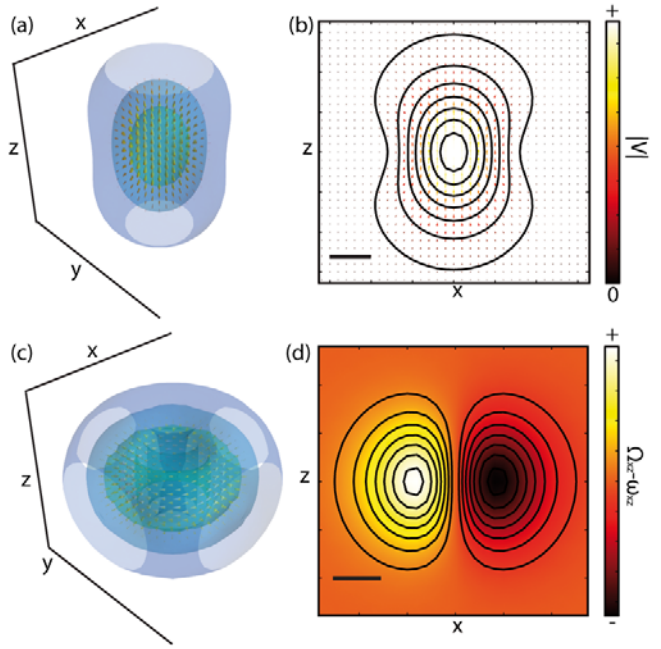

Fig. 3. Flow $\mathbf{v}$ and rotation field $\boldsymbol{\Omega} - \boldsymbol{\omega}$ of the polar ring motors (fig. 1(b) and (c)). The velocity field $\mathbf{v}$ is shown in (a), where velocity vectors as well as surfaces of constant $|\mathbf{v}|$ are indicated. The flow in the (x, z)-plane for $y = 0$ is shown in (b). The rotation field of the polar ring motor is shown in (c) and (d). The rotation vectors $\boldsymbol{\Omega} - \boldsymbol{\omega}$ are indicated as cones and surfaces of constant magnitude are also indicated. Cross-sections in the (x, z)-plane at $y = 0$ are shown in (d). The black scale bar indicates the length ℓ. The parameters are $\eta/\eta' = 1$. The size of the periodic box is 26ℓ.

4.1.4 Polar ring motor

The polar ring motor is defined by ζ_4 and $\tilde{\zeta} = \zeta_1 = \zeta_2 = \zeta_3 = 0$. Unlike the other motors we discussed, this motor is not chiral. We determine the velocity field and the intrinsic rotation field of the polar ring motor numerically. The velocity field is displayed in fig. 3(a), (b). The motor generates a velocity field $\mathbf{v}$ that does not vanish in the limit of small r. This implies that the polar ring motor is a swimmer, which propels itself in the direction set by the vector $\mathbf{p}$. The polar ring motor generates a velocity far field in the limit $\ell \to 0$ that can be determined analytically

$$v_\alpha \simeq \frac{\zeta_4 \Delta\mu_0}{8\pi\eta} \left(\frac{3 r_\alpha}{|\mathbf{r}|^5} \mathbf{r} \cdot \mathbf{p} - p_\alpha \frac{1}{|\mathbf{r}|^3} \right). \tag{42}$$

The polar ring motor also generates intrinsic rotations. The field of intrinsic rotations is $\Omega_{\alpha\beta} \neq \omega_{\alpha\beta}$ in the near field, $r \ll \ell$, and becomes equal to the vorticity in the far-field, $r \gg \ell$, see fig. 3(c), (d).

4.2 Ensembles of chiral motors

We now discuss an example of spontaneous flows created by an ensemble of active chiral motors. We consider an active chiral fluid confined between two solid surfaces in the (x, y)-plane at distance d, see fig. 4(a). We choose no-slip boundary conditions and impose vanishing rotation fields, $\Omega_{\alpha\beta} = 0$, on both surfaces. We assume the lower surface at $z = 0$ to be immobile, $\mathbf{v}(z = 0) = 0$. The upper surface moves at velocity $\Delta\mathbf{v}$ in the y-direction, $\mathbf{v}(z = d) = \Delta v \hat{\mathbf{e}}_y$. We choose the direction of the polarity $\mathbf{p}$ on both surfaces to point parallel to the surface in the x-direction. The polarity field is governed by a free-energy functional that is minimized if the polarity $\mathbf{p}$ is locally aligned and we impose the constraint $|\mathbf{p}| = 1$.

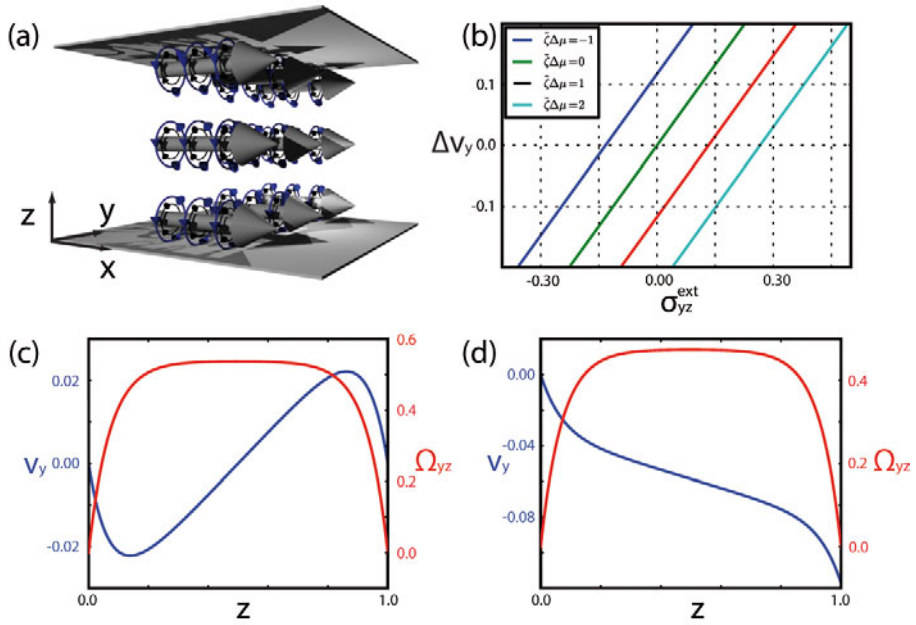

Fig. 4. Chiral shear flows generated by active chiral processes with a constant polarity vector, enclosed between two surfaces of distance d. (a) Schematic representation of the system. (b) Velocity difference Δv_y between upper and lower plate as a function of external shear stress $\sigma_{zy}^{\rm ext}$, applied to the surfaces for difference values of the parameter $\tilde{\zeta}\Delta\mu$. (c) Profile of velocity v_y and rotation rate Ω_{yz} as a function of position z between the plates for fixed plates, $\Delta\mathbf{v}=0$. (d) Profile of velocity v_y and rotation rate Ω_{yz} as a function of position z between the plates for $\sigma_{zy}^{\rm ext}=0$. Parameter values are $\tilde{\zeta}\Delta\mu=1$, $\eta/\eta'=1$ and $\ell/d=0.1$.

We first assume $\mathbf{p}=\hat{\mathbf{e}}_x$ also in the volume. Using eqs. (33) and (34), we then find $\Omega_{xz}=\Omega_{xy}=0$ and $v_x=v_z=0$. The velocity v_y and the intrinsic rotation rate Ω_{yz} obey

$$(\eta+\eta')\partial_z^2 v_y+2\eta'\partial_z\Omega_{yz}=0, \tag{43}$$

$$(\kappa_0\partial_z^2-4\eta')\Omega_{yz}-2\eta'\partial_z v_y-2\tilde{\zeta}\Delta\mu=0. \tag{44}$$

The dynamics of the polarity $\mathbf{p}$ is given by

$$\partial_t p_\alpha=\frac{1}{\gamma}h_\alpha^{\rm tot}-v_\gamma\partial_\gamma p_\alpha-\Omega_{\alpha\beta}p_\beta. \tag{45}$$

Because for constant $\mathbf{p}=\hat{\mathbf{e}}_x$, $\mathbf{h}^{\rm tot}=0$ and thus $\mathbf{p}$ is stationary. The active fluid exerts a wall shear stress,

$$\sigma_{yz}^{\rm tot}|_{z=d}=\left\{(\eta+\eta')\partial_z v_y+\tilde{\zeta}\Delta\mu\right\}\big|_{z=d}. \tag{46}$$

Figure 4(b) shows the profiles of velocity v_y and intrinsic rotation rate Ω_{zy} obtained by the numerical solution of eqs. (33) and (34) as a function of z/d for two immobile plates, $\Delta\mathbf{v}=0$.

For the boundary condition $\sigma_{yz}^{\rm tot}|_{z=d}=0$, *i.e.* no shear stress between the plates, the plates move relative to each other, *i.e.* $\Delta\mathbf{v}\neq 0$. The flow profile for this boundary condition is displayed in fig. 4(d). The system acts as a motor because $\Delta\mathbf{v}$ depends linearly on the imposed shear stress. The resulting stress-velocity relationships for different values of $\tilde{\zeta}\Delta\mu$ are displayed in fig. 4(c). Note that it is the polar chiral term $\tilde{\zeta}$ that generates this relative motion of the plates. Interestingly, even though an individual polar chiral motor does not generate a far field, homogeneous distributions of such motors create relative flows at large separation. These flows are created in a thin boundary layer. The stress between the plates does not depend on d for $\ell\ll d$.

5 Summary and discussion

Our study of active chiral fluids is related to earlier work on the physics of passive liquid crystals with chiral asymmetry such as cholesterics, where passive chiral terms govern chiral effects in the fluid [47]. However, here we ignore passive chiral effects for simplicity and focus on the physics of active chiral processes, which we expect to be dominant in biological systems. We have presented a generic theory for complex fluids in which active processes with chiral asymmetry drive the non-equilibrium dynamics. In such a fluid the chiral asymmetry of the active processes generates active chiral force and torque dipoles. Such force and torque dipoles give rise to active contributions to antisymmetric stresses and to angular momentum fluxes, which can be described by elementary chiral motors.

Following previous work on intrinsic rotations in liquid crystals [49], our theory accounts for angular momentum fluxes and describes both the center-of-mass velocity field as well as the field of intrinsic rotations. In the presence of active chiral processes, the intrinsic rotation can differ from the vorticity of the flow even in steady state, while in passive fluids both become equal after a relaxation time, which usually is short [49]. This effect, however, only exists within a length scale ℓ and therefore disappears in the hydrodynamic limit.

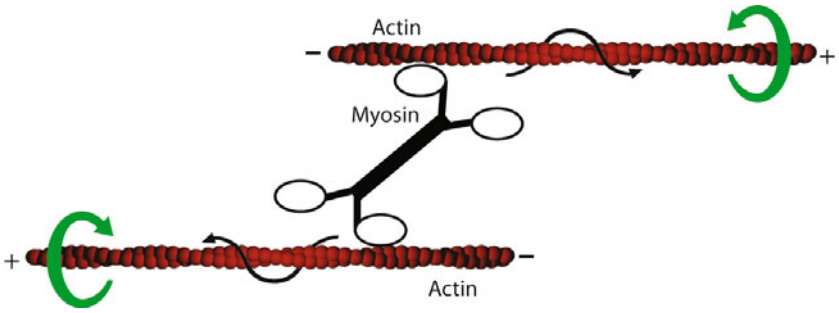

Fig. 5. Sketch of a cytoskeletal torque dipole showing a myosin mini-filament (black and white) acting between two antiparalel actin filaments (red). The motor-heads walk along the actin filaments following a helical path (black arrows). This induces counter-rotations of the two actin filaments and gives rise to two opposed torque monopoles exerted on the fluid (green curved arrows).

We identified four types of elementary chiral motors generated by distributions of chiral force and torque dipoles. These motors differ by their near and far fields: (a) isotropic chiral motors, (b) chiral rods, (c) chiral rings and (e) polar chiral motors. Isotropic motors (a) generate a field of local intrinsic rotations but no flow field. This rotation field decays on the length scale ℓ. Chiral rods (b) and rings (c) both have nematic symmetry. They generate the same hydrodynamic far field with a velocity that decays as $\mathbf{v} \sim |\mathbf{r}|^{-3}$. Their intrinsic rotation fields differ at short distances but become both equal to the vorticity of $\mathbf{v}$ in the far field. The polar chiral motor (e) does not generate a hydrodynamic far field but both a flow and a intrinsic rotation field at short distances. We also showed that a related non-chiral polar ring motor (d) is a swimmer that generates a hydrodynamic far field.

Active processes resulting from a homogeneously distributed collection of aligned polar chiral motors introduce an active contribution to antisymmetric stresses that is constant throughout the fluid. Interestingly, even though individual polar chiral motors do not generate a hydrodynamic far field, a collection at sufficient density gives rise to flow at large distance from a surface, induced by a boundary layer of thickness ℓ. As a result, an active chiral fluid with polar order confined between two plates can generate spontaneous relative motion of the plates and shear stresses between the plates, see fig. 4. The direction of the motion Δv is proportional to $\mathbf{p} \times \mathbf{n}$, where $\mathbf{n}$ is the vector normal to the plate. We have shown that the stresses on the plates are linear in the density of chiral motors and do not depend on the distance between plates for $\ell \ll d$.

The main motivation of this study of active chiral processes in soft matter is the cell cytoskeleton. In particular the actin-myosin networks in cells form dense cross-linked gels for which the continuum approach developed here is well suited to describe large-scale dynamics [19]. Because actin filaments are helical objects, the interaction between actin and myosin is chiral. This is most clearly seen in gliding assays where myosin heads are attached to a substrate. Myosin motors set actin filaments in motion. In addition to translation, it was shown that actin filaments also rotate [26]. This implies that the motor performs a helical movement on the filament while translocating. The helical trajectory of the motor with respect to the filament can be described by a radius r and a pitch p. Such a helical movement of motors gives rise to a counter-rotation of two filaments which interact via a myosin mini-filament, see fig. 5. The relative sliding of filaments implies the existence of a force dipole, while the counter-rotation implies the existence of a torque dipole. We estimate this torque dipole using eq. (8). The magnitude of the torque dipole is $aq \simeq 2\pi f a r^2/(4\pi^2 r^2 + p^2)^{1/2}$. Here, a is the distance between the filaments, f is a characteristic motor force, r is the radius of the myosin trajectory (estimated as the radius of the actin filament) and p is the pitch of the helical path of the myosin along the actin.

If we assume for simplicity that the motor follows the helical pitch of the actin filament structure, we estimate $p \simeq 72\,\mathrm{nm}$. Using $f \simeq 10\,\mathrm{pN}$, $r \simeq 5\,\mathrm{nm}$ and $a \simeq 100\,\mathrm{nm}$, we estimate $qa \simeq 10^{-27}\,\mathrm{N\,m^2}$. We can now estimate the magnitude of the active angular momentum fluxes described by the coefficients $\zeta_i \Delta\mu$ with $i = 1 \ldots 4$ in eq. (25), as $\zeta_i \Delta\mu \simeq aqc$. Here c denotes the torque dipole density. Using $c \simeq a^{-3}$, which corresponds to an actin network with a mesh size of $a \simeq 100\,\mathrm{nm}$, we have $\zeta_i \Delta\mu \simeq 10^{-6}\,\mathrm{N/m}$. In addition to active contributions to angular momentum fluxes, active chiral processes also contribute to antisymmetric stresses with magnitude $\tilde{\zeta}\Delta\mu$. Generalizing our arguments, we find $\tilde{\zeta}\Delta\mu \simeq qc$, which leads to the estimate $\tilde{\zeta}\Delta\mu \simeq 10\,\mathrm{N/m^2}$. The ratio of the magnitudes of active antisymmetric stresses and non-chiral active stresses can be estimated as $\tilde{\zeta}\Delta\mu/(\zeta\Delta\mu) \simeq q/(fa)$, which in the limit of small pitch p approaches r/a. Therefore, in dense gels with small pitches of myosin motion, effects of active chiral processes could become substantial. The value of p in actin-myosin gels depends in general on the particular myosin motor used could vary widely. Note that in living cells additional proteins that interact with actin and/or myosin could regulate the key parameters, such as r and p, giving rise to active chiral effects. Finally, the characteristic length scale ℓ introduced in eq. (37) is a microscopic length which in actin gels we expect to be of the of the order of the mesh size $a \simeq 100\,\mathrm{nm}$.

Other examples of active chiral systems are provided by suspensions of chiral swimmers. An important example are bacteria such as *E. coli*, which consists of a cell body to which about $N = 10$ rotating flagella are attached.

This rotation is generated by rotational motors embedded in the cell membrane. The stall torque of these motors is of the order $q \simeq 10^{-18}\,\mathrm{N\,m}$, see [11, 51]. For a freely swimming bacterium, the torque is smaller and set by hydrodynamic friction. The bacterium therefore is a torque dipole of strength Nqa, where $a \simeq 1$ μm is the typical size of the bacterium [1, 11]. Knowing the torque q and the bacterium density c, one can estimate the magnitudes of the angular momentum fluxes in a suspension of such bacteria as $\zeta_i \Delta\mu \simeq Nqac$ as well as of the antisymmetric stress $\tilde{\zeta}\Delta\mu \simeq Nqc$. The characteristic length scale ℓ is expected to be of the order of the bacterium size a.

The active chiral effects we predict could in principle be observed experimentally using the setup sketched in fig. 4 using acto-myosin gel with polar order or an ordered suspension of swimming bacteria. The stress $\sigma^{\mathrm{tot}}_{yz}$ exerted on the surfaces due to active chiral processes is of the order $\tilde{\zeta}\Delta\mu$ estimated above, see eq. (46). This example also illustrates that chiral effects become most prominent near surfaces. In fact, active chiral processes have usually been observed experimentally near walls or surfaces. For instance, chiral flows are seen in chiral granular gases driven by a vibrating surface [24]. Moreover, many examples of thin films of chiral active fluids are found in biology. During development, these are often tightly connected with the breakage of left-right symmetry in organisms [37]. For instance, surfaces covered with beating cilia, which often exhibit a rotating component in their beating motion can be described as chiral rods attached to a solid substrate [32, 33]. Such cilia play a key role in the left-right symmetry breaking of the morphology of developing embryos [34, 35]. Another example of a thin active chiral film is the actomyosin cell cortex, which is a thin film of active material below the cell membrane [19]. This chirality becomes evident in chiral movements on the cell cortex such as for instance in the fertilized egg of the frog *Xenopus* [52]. Interestingly, the chiral motion of the cell cortex, can generate active torque dipoles on the level of tissues which are involved in the left-right symmetry breakage of snails [53] and *C. elegans* [54]. Finally *E. Coli* attached to a surface have been shown to generate chiral flows [55]. A logical extension of the work presented here would be a theory of thin films of active chiral fluids, which is the subject of a separate publication [56].

Finally, while in simple fluids the characteristic length ℓ on which intrinsic rotations matter is of a microscopic scale, in biological systems such as the cytoskeleton this length can be significant. Therefore, we expect that the field of intrinsic rotations is relevant for such systems and gives rise to new physics even on long time scales.

Appendix A. The Ericksen stress

Consider the variation of the free energy,

$$\delta F = \int_{\partial V} \left[f u_\alpha \delta_{\alpha\beta} + \frac{\partial f_0}{\partial(\partial_\beta p_\gamma)} \delta p_\gamma \right] \mathrm{d}S_\beta + \int_V \mathrm{d}x^3 \left[v_\alpha \delta g_\alpha + \Omega_\alpha \delta l_\alpha - h^{\mathrm{tot}}_\alpha \delta p_\alpha + \mu^{\mathrm{tot}} \delta n \right], \quad \text{(A.1)}$$

where vector $\mathbf{u}$ describes an infinitesimal displacement of the boundary. If $\delta g_\alpha = -u_\gamma \partial_\gamma g_\alpha$ and alike for δp_α, δl_α and δn, δF is the free-energy change under a distortion of the volume V and reads

$$\begin{aligned}\delta F = \int_{\partial V} \Big\{ & (f - n\mu^{\mathrm{tot}} - g_\gamma v_\gamma - l_\gamma \Omega_\gamma)\delta_{\alpha\beta} \\ & - \frac{\partial f}{\partial(\partial_\beta p_\gamma)} \partial_\alpha p_\gamma \Big\} u_\alpha \mathrm{d}S_\beta + \int_V \mathrm{d}x^3 u_\gamma \big(g_\alpha \partial_\gamma v_\alpha \\ & + l_\alpha \partial_\gamma \Omega_\alpha + h^{\mathrm{tot}}_\alpha \partial_\gamma p_\alpha + n \partial_\gamma \mu^{\mathrm{tot}} \big) \\ & + \int_V \mathrm{d}x^3 \left(\mu^{\mathrm{tot}} n + g_\alpha v_\alpha + l_\gamma \Omega_\gamma \right) \partial_\gamma u_\gamma. \end{aligned} \quad \text{(A.2)}$$

The Ericksen stress is given by the surface term eq. (14). As a consequence of translation invariance the left-hand side of eq. (A.2) vanishes for constant $\mathbf{u}$. This leads to the Gibbs-Duhem relation eq. (15). Finally, since the free energy is invariant under rotations by an infinitesimal angle θ, the left-hand side of eq. (A.2) also vanishes if $u_\alpha = \epsilon_{\alpha\beta\gamma}\theta_\beta r_\gamma$, $\delta p_\alpha = -u_\gamma \partial_\gamma p_\alpha + \epsilon_{\alpha\beta\gamma}\theta_\beta p_\gamma$, $\delta l_\alpha = -u_\gamma \partial_\gamma l_\alpha + \epsilon_{\alpha\beta\gamma}\theta_\beta l_\gamma$, $\delta g_\alpha = -u_\gamma \partial_\gamma g_\alpha + \epsilon_{\alpha\beta\gamma}\theta_\beta g_\gamma$ and $\delta n = 0$. This leads to eq. (16).

Appendix B. The entropy production rate

We derive the entropy production rate of a fluid with k components. Equation (A.1) is easily generalized to the multi-component case. We consider the variation where $\delta F = \dot{F}\delta t$, $u_\gamma = v_\gamma \delta t$, $\delta g_\alpha = \partial_t g_\alpha \delta t$, $\delta l_\alpha = \partial_t l_\alpha \delta t$, $\delta p_\alpha = \partial_t p_\alpha \delta t$ and $\delta n_i = \partial_t n_i \delta t$. Here n_i denotes the number density of the i-th component of the fluid. In this case

$$\begin{aligned}\dot{F} = & \int_{\partial V} \left[f v_\alpha \delta_{\alpha\beta} + \frac{\partial f_0}{\partial(\partial_\beta p_\gamma)} \partial_t p_\gamma \right] \mathrm{d}S_\beta \\ & + \int_V \mathrm{d}x^3 \Big[v_\alpha \partial_t g_\alpha + \frac{1}{2}\Omega_{\alpha\beta}\partial_t l_{\alpha\beta} - h^{\mathrm{tot}}_\alpha \partial_t p_\alpha \\ & + \sum_i \mu^{\mathrm{tot}}_i \partial_t n_i \Big]. \end{aligned} \quad \text{(B.1)}$$

Using the force balance (1), the Gibbs Duhem relation (15) and performing a partial integration

$$\begin{aligned}\dot{F} = & \int_{\partial V} \Big[f v_\alpha \delta_{\alpha\beta} + \frac{\partial f_0}{\partial(\partial_\beta p_\gamma)} \partial_t p_\gamma \\ & + \Big\{ \sigma^{\mathrm{tot}}_{\alpha\beta} - \sigma^e_{\alpha\beta} - \sum_i (n_i \mu^{\mathrm{tot}}_i + \Omega_\gamma l_\gamma)\delta_{\alpha\beta} \Big\} v_\alpha \Big] \mathrm{d}S_\beta \\ & + \int_V \mathrm{d}x^3 \Big[v_\alpha \phi^{\mathrm{ext}}_\alpha - \Big(\sigma^{\mathrm{tot}}_{\alpha\beta} - \sigma^e_{\alpha\beta} + g_\alpha v_\beta \\ & - \sum_i n_i \mu^{\mathrm{tot}}_i \delta_{\alpha\beta} \Big) \partial_\beta v_\alpha + \frac{1}{2}\Omega_{\alpha\beta}(\partial_t l_{\alpha\beta} + \partial_\gamma (l_{\alpha\beta} v_\gamma)) \\ & - h^{\mathrm{tot}}_\alpha \frac{\mathrm{d}}{\mathrm{d}t} p_\alpha + \sum_i \mu^{\mathrm{tot}}_i \frac{\mathrm{d}}{\mathrm{d}t} n_i \Big]. \end{aligned} \quad \text{(B.2)}$$

The particle number conservation is given by

$$\partial_t n_i = -\partial_\alpha \left(n_i v_\alpha + \frac{j^i_\alpha}{m_i} \right) + R_i, \tag{B.3}$$

where $\mathbf{j}^i$ are the dissipative particle fluxes, m_i are the particle masses and R_i are particle source terms, which describe chemical reactions between the fluid components. We introduce $\bar{\mu_i} = (\mu_i^{\rm tot} m_k - \mu_k^{\rm tot} m_i)/(m_i m_k)$ and separate the stress into a symmetric and an antisymmetric part, writing that

$$\begin{aligned}\left(\sigma^{\rm tot}_{\alpha\beta} - \sigma^{e}_{\alpha\beta}\right)\partial_\beta v_\alpha = &\left\{\sigma^{\rm tot}_{\alpha\beta} - \sigma^{{\rm tot},a}_{\alpha\beta} - \left(\sigma^{e}_{\alpha\beta} - \sigma^{e,a}_{\alpha\beta}\right)\right\} u_{\alpha\beta} \\ &- \left(\sigma^{{\rm tot},a}_{\alpha\beta} - \sigma^{e,a}_{\alpha\beta}\right)\omega_{\alpha\beta}.\end{aligned} \tag{B.4}$$

Using the particle number conservation (B.3), the torque balance (3), eq. (16) and that $\sum_{i=1}^k \mathbf{j}^i = 0$ by definition, we find

$$\begin{aligned}\dot{F} = \int_{\partial V} \Big[& f v_\alpha \delta_{\alpha\beta} + \frac{\partial f_0}{\partial(\partial_\beta p_\gamma)} \partial_t p_\gamma + \big(\sigma^{\rm tot}_{\alpha\beta} - \sigma^{e}_{\alpha\beta} \\ & - \big(n_i \mu_i^{\rm tot} + \Omega_\gamma l_\gamma\big)\delta_{\alpha\beta}\big) v_\alpha + \frac{1}{2}\Omega_{\alpha\delta}\big\{M^{\rm tot}_{\alpha\beta\gamma} - M^{e}_{\alpha\beta\gamma} \\ & - \big(r_\alpha \sigma^{\rm tot}_{\beta\gamma} - r_\beta \sigma^{\rm tot}_{\alpha\gamma}\big) + l_{\alpha\beta} v_\gamma\big\} - j^i_\beta \frac{\mu_i^{\rm tot}}{m_i}\Big] {\rm d}S_\beta \\ & + \int_V {\rm d}x^3 \left(\frac{1}{2}\Omega_{\alpha\beta}\tau^{\rm ext}_{\alpha\beta} + v_\alpha \phi^{\rm ext}_\alpha \right) \\ & + \int_V {\rm d}x^3 \Big[- \big\{\sigma^{\rm tot}_{\alpha\beta} - \sigma^{{\rm tot},a}_{\alpha\beta} - \big(\sigma^{e}_{\alpha\beta} - \sigma^{e,a}_{\alpha\beta}\big) + g_\alpha v_\beta\big\} u_{\alpha\beta} \\ & - \left(\sigma^{{\rm tot},a}_{\alpha\beta} - \sigma^{e,a}_{\alpha\beta}\right)\left(\Omega_{\alpha\beta} - \omega_{\alpha\beta}\right) \\ & - \frac{1}{2}\left\{M^{\rm tot}_{\alpha\beta\gamma} - M^{e}_{\alpha\beta\gamma} - \big(r_\alpha \sigma^{\rm tot}_{\beta\gamma} - r_\beta \sigma^{\rm tot}_{\alpha\gamma}\big) + l_{\alpha\beta} v_\gamma\right\} \\ & \times \partial_\gamma \Omega_{\alpha\beta} - h^{\rm tot}_\alpha \left(\frac{\rm d}{{\rm d}t} p_\alpha + \Omega_{\alpha\beta} p_\beta \right) \\ & + \sum_{i=1}^{k-1} j^i_\alpha \partial_\alpha \bar{\mu}_i + R_i \mu_i^{\rm tot} \Big].\end{aligned} \tag{B.5}$$

We are thus to identify the free-energy flux over the boundaries

$$\begin{aligned}-J^{(F)}_\beta = & f v_\alpha \delta_{\alpha\beta} + \frac{\partial f_0}{\partial(\partial_\beta p_\gamma)} \partial_t p_\gamma + \big(\sigma^{\rm tot}_{\alpha\beta} - \sigma^{e}_{\alpha\beta} \\ & - (n_i \mu_i^{\rm tot} + \Omega_\gamma l_\gamma)\delta_{\alpha\beta}\big) v_\alpha \\ & + \frac{1}{2}\Omega_{\alpha\delta}\Big\{M^{\rm tot}_{\alpha\beta\gamma} - M^{e}_{\alpha\beta\gamma} - \big(r_\alpha \sigma^{\rm tot}_{\beta\gamma} - r_\beta \sigma^{\rm tot}_{\alpha\gamma}\big) \\ & + l_{\alpha\beta} v_\gamma\Big\} - j^i_\beta \frac{\mu_i^{\rm tot}}{m_i},\end{aligned} \tag{B.6}$$

the rate of work performed on the system

$$\dot{W} = \int_V {\rm d}x^3 \left(\frac{1}{2}\Omega_{\alpha\beta}\tau^{\rm ext}_{\alpha\beta} + v_\alpha \phi_\alpha \right), \tag{B.7}$$

and the entropy production rate

$$\begin{aligned}T\dot{\Theta} = \int {\rm d}x^3 \Big\{ & \sigma_{\alpha\beta} u_{\alpha\beta} + \sigma^a_{\alpha\beta}(\Omega_{\alpha\beta} - \omega_{\alpha\beta}) \\ & + \frac{1}{2} M_{\alpha\beta\gamma}\partial_\gamma \Omega_{\alpha\beta} + h^{\rm tot}_\alpha \frac{D}{Dt} p_\alpha \\ & - \sum_{i=1}^{k-1} j^i_\alpha \partial_\alpha \bar{\mu}_i - \mu_i^{\rm tot} R_i \Big\}.\end{aligned} \tag{B.8}$$

To recover eq. (18) we consider a three-component system consisting of the gel, the fuel molecules and their reaction products. If the concentrations of fuel and reaction products are kept constant by contact with an external buffer $\mathbf{j}^i = 0$ and $\mu_i^{\rm tot} R^i$ can be rewritten as $r\Delta\mu$, where $r = R_{\rm product} = -R_{\rm fuel}$ and $\Delta\mu = \mu^{\rm tot}_{\rm fuel} - \mu^{\rm tot}_{\rm product}$.

Appendix C. The Newtonian fluid

The constitutive equations for the Newtonian fluid are

$$\begin{aligned}\sigma_{\alpha\beta} &= 2\eta u_{\alpha\beta}, \\ \sigma^a_{\alpha\beta} &= 2\eta' \left(\Omega_{\alpha\beta} - \omega_{\alpha\beta}\right), \\ M_{\alpha\beta\gamma} &= \kappa_0 \partial_\gamma \Omega_{\alpha\beta}.\end{aligned} \tag{C.1}$$

The equations of motion (28) and (29) then read

$$\begin{aligned}\partial_t g_\alpha + \partial_\beta (v_\beta g_\alpha) = & 2\eta \partial_\beta u_{\alpha\beta} \\ & + 2\eta' \partial_\beta \left(\Omega_{\alpha\beta} - \omega_{\alpha\beta}\right) - \partial_\alpha P\end{aligned} \tag{C.2}$$

and

$$\partial_t l_{\alpha\beta} + \partial_\gamma (v_\gamma l_{\alpha\beta}) = \kappa_0 \partial^2_\gamma \Omega_{\alpha\beta} - 4\eta' \left(\Omega_{\alpha\beta} - \omega_{\alpha\beta}\right), \tag{C.3}$$

respectively, where we used the fact that the moment of inertia tensor is diagonal for the Newtonian fluid. Moreover the fluid is incompressible, such that

$$\partial_\alpha v_\alpha = 0. \tag{C.4}$$

If we finally use that the moment of inertia tensor is isotropic in the Newtonian fluid $l_{\alpha\beta} = I\Omega_{\alpha\beta}$ and find

$$\begin{aligned}\frac{{\rm d}g_\alpha}{{\rm d}t} = & \eta \partial^2_\gamma v_\alpha - \partial_\alpha P + \frac{\kappa_0}{4\eta'} \left(\partial^2_\gamma - \frac{I}{\kappa_0}\frac{\rm d}{{\rm d}t} \right) \\ & \times \left[\frac{{\rm d}g_\alpha}{{\rm d}t} - (\eta + \eta')\partial^2_\gamma v_\alpha + \partial_\alpha P \right],\end{aligned} \tag{C.5}$$

For $\kappa_0 \to 0$ eq. (C.5) becomes the Navier-Stokes equation. On length large comparated to the characteristic length $\ell = \sqrt{\kappa_0/\eta'}$ and times long compared to $\tau = I/\eta'$, the additional terms related to the dissipative coefficients κ_0 and η' can be neglected. In a passive Newtonian fluid the dissipative contributions to the antisymmetric stress and to $M_{\alpha\beta\gamma}$ become irrelevant in the hydrodynamic limit.

Appendix D. Elimination of antisymmetric stresses by variable changes

In the absence of bulk torques, the antisymmetric stress can be eliminated using a variable change [46]. This result is based on the invariance of mass conservation equation $\partial_t \rho = -\partial_\alpha g_\alpha$, under a redefinition of the momentum density

$$\tilde{g}_\alpha = g_\alpha + \frac{1}{2}\partial_\beta l_{\alpha\beta}, \tag{D.1}$$

that also obeys

$$\partial_t \rho = -\partial_\alpha \tilde{g}_\alpha. \tag{D.2}$$

The momentum density $\tilde{\mathbf{g}}$ is also conserved

$$\partial_t \tilde{g}_\alpha = \partial_\beta \tilde{\sigma}^{\rm tot}_{\alpha\beta}, \tag{D.3}$$

where

$$\begin{aligned}\tilde{\sigma}^{\rm tot}_{\alpha\beta} &= \sigma^{\rm tot}_{\alpha\beta} - \frac{1}{2}(\partial_\gamma M^\pi_{\alpha\beta\gamma} - \partial_t l_{\alpha\beta}) \\ &\quad + \frac{1}{2}\partial_\gamma \left(M^\pi_{\alpha\gamma\beta} + M^\pi_{\beta\gamma\alpha}\right) \qquad \text{(D.4)} \\ &= \sigma^{\rm tot}_{\alpha\beta} - \sigma^{{\rm tot},a}_{\alpha\beta} + \frac{1}{2}\partial_\gamma \left(M^\pi_{\alpha\gamma\beta} + M^\pi_{\beta\gamma\alpha}\right) \qquad \text{(D.5)}\end{aligned}$$

is symmetric by definition. The coarse-grained kinetic free energy density,

$$f - f_0 = \frac{\mathbf{g}^2}{2\rho} + \frac{1}{2} I^{-1}_{\alpha\beta} l_\alpha l_\beta, \tag{D.6}$$

implies that the momentum density $\mathbf{g}$ and the angular momentum density $\mathbf{l}$ can be defined uniquely within each coarse-graining volume element. Note that this coarse-grained free-energy density is not invariant with respect to replacing $\mathbf{g}$ by $\tilde{\mathbf{g}}$ and also $f - f_0 \neq \tilde{\mathbf{g}}^2/(2\rho)$. It follows from these arguments that the hydrodynamic problem can be expressed in terms of new variables such that the stress tensor $\tilde{\sigma}_{\alpha\beta}$ is symmetric. However the entropy production rate (18) as well as the constitutive equations (23)–(27) do not change, and the physics remains exactly the same. In particular the phenomenological coefficients of eqs. (24) and (25) also occur in a representation in which stresses are symmetric.

References

1. D. Bray, *Cell Movements*, 2nd edition (Garland Pub., 2000).
2. J. Howard, *Mechanics of Motor Proteins and the Cytoskeleton* (Palgrave Macmillan, 2001).
3. T. Mitchison, L. Cramer, Cell **84**, 371 (1996).
4. S.W. Grill, J. Howard, E. Schaffer, E.H. Stelzer, A. Hyman, Science **301**, 518 (2003).
5. A. Zumdieck, M.C. Lagomarsino, C. Tanase, K. Kruse, B. Mulder, M. Dogterom, F. Jülicher, Phys. Rev. Lett. **95**, 258103 (2005).
6. J. Pecreaux, J.-C. Röper, K. Kruse, F. Jülicher, A. Hyman, S.W. Grill, J. Howard, Curr. Biol. **16**, 2111 (2006).
7. G. Salbreux, J. Prost, J.-F. Joanny, Phys. Rev. Lett. **103**, 058102 (2009).
8. I.R. Gibbons, J. Cell Biol. **91**, 107 (1981).
9. A. Hilfinger, F. Jülicher, Phys. Biol. **5**, 016003 (2008).
10. E. Purcell, Am. J. Phys. **45**, 3 (1977).
11. H.C. Berg, *E. Coli in Motion* (Springer-Verlag, New York, 2004).
12. R. Foty, G. Forgacs, C. Pfleger, M. Steinberg, Phys. Rev. Lett. **72**, 2298 (1994).
13. J. Ranft, M. Basan, J. Elgeti, J.-F. Joanny, J. Prost, F. Jülicher, Proc. Natl. Acad. Sci. U.S.A. **107**, 20863 (2010).
14. R. Aditi Simha, S. Ramaswamy, Phys. Rev. Lett. **83**, 058101 (2002).
15. R. Voituriez, J.-F. Joanny, J. Prost, Europhys. Lett. **70**, 404 (2005).
16. S. Fürthauer, M. Neef, S.W. Grill, K. Kruse, F. Jülicher, New J. Phys. **14**, 023001 (2012).
17. Y. Hatwalne, S. Ramaswamy, M. Rao, R.A. Simha, Phys. Rev. Lett. **92**, 118101 (2004).
18. F. Jülicher, K. Kruse, J. Prost, J.-F. Joanny, Phys. Rep. **449**, 3 (2007).
19. M. Mayer, M. Depken, J. Bois, F. Jülicher, S.W. Grill, Nature **467**, 617 (2010).
20. C. Dombrowski, L. Cisneros, L. Chatkaew, R. Goldstein, J. Kessler, Phys. Rev. Lett. **93**, 098103 (2004).
21. A. Baskarana, M.C. Marchetti, Proc. Natl. Acad. Sci. U.S.A. **106**, 15569 (2009).
22. M. Basan, J.-F. Joanny, J. Prost, T. Risler, Phys. Rev. Lett. **106**, 158101 (2011).
23. L. Bocquet, W. Losert, D. Schalk, T.C. Lubensky, J.P. Gollub, Phys. Rev. E **65**, 011307 (2001).
24. J.-C. Tsai, F. Ye, J. Rodriguez, J.P. Gollub, T.C. Lubensky, Phys. Rev. Lett. **94**, 214301 (2005).
25. I.S. Aranson, L.S. Tsimring, Rev. Mod. Phys. **78**, 641 (2006).
26. I. Sase, H. Miyata, S. Ishiwata, K. Kinosita Jr, Proc. Natl. Acad. Sci. U.S.A. **94**, 5646 (1997).
27. M. Lenz, F. Jülicher, J.-F. Joanny, J. Prost, Phys. Rev. Lett. **91**, 108104 (2003).
28. A. Vilfan, Biophys. J. **97**, 1130 (2009).
29. M. Leoni, T.B. Liverpool, EPL **92**, 64004 (2010).
30. Y. Fily, A. Baskaran, M.C. Marchetti, Soft Matter **8**, 3002 (2012).
31. R. Di Leonardo, D. Dell'Arciprete, L. Angelani, V. Iebba, Phys. Rev. Lett. **106**, 038101 (2011).
32. J. Buceta, M. Ibañes, D. Rasskin-Gutman, Y. Okada, N. Hirokawa, J.C. Izpisúa-Belmontey, Biophys. J. **89**, 2199 (2005).
33. D.J. Smith, J.R. Blake, E.A. Gaffney, J. R. Soc. Interface **5**, 567 (2008).
34. S. Nonaka, Y. Tanaka, Y. Okada, S. Takeda, A. Harada, Y. Kanai, M. Kido, N. Hirokawa, Cell **95**, 829 (1998).
35. S. Nonaka, S. Yoshiba, D. Watanabe, S. Ikeuchi, T. Goto, W.F. Marshall, H. Hamada, PLoS Biol. **3**, e268 (2005).
36. L.N. Vandenberg, L. Levin, Semin. Cell Develop. Biol. **20**, 456 (2009).

37. C.L. Henley, arXiv:0811.0055v2 (2008).
38. C.L. Henley, arXiv:1112.2317v1 (2011).
39. J.H.E. Cartwright, O. Piro, I. Tuva, Proc. Natl. Acad. Sci. U.S.A. **101**, 7234 (2004).
40. T.B. Liverpool, M.C. Marchetti, Europhys. Lett. **69**, 84 (2005).
41. K. Kruse, F. Jülicher, Phys. Rev. Lett. **85**, 1778 (2000).
42. K. Kruse, J.-F. Joanny, F. Jülicher, J. Prost, K. Sekimoto, Phys. Rev. Lett. **92**, 078101 (2004).
43. K. Kruse, J.-F. Joanny, F. Jülicher, J. Prost, K. Sekimoto, Eur. Phys. J. E **16**, 5 (2005).
44. J.-F. Joanny, F. Jülicher, K. Kruse, J. Prost, New J. Phys. **9**, 422 (2007).
45. S.R. de Groot, P. Mazur, *Non-Equilibrium Thermodynamics* (Dover Pub., 1984).
46. P.C. Martin, O. Parodi, P.S. Pershan, Phys. Rev. A **6**, 6 (1972).
47. P.G. de Gennes, J. Prost, *The Physics of Liquid Crystals* (Oxford University Press, 1995).
48. H. Stark, T.C. Lubensky, Phys. Rev. E **67**, 061709 (2003).
49. H. Stark, T.C. Lubensky, Phys. Rev. E **72**, 051714 (2005).
50. K. Drescher, K.C. Leptos, I. Tuval, T. Ishikawa, T.J. Pedley, R.E. Goldstein, Phys. Rev. Lett. **102**, 168101 (2009).
51. R.M. Berry, H.C. Berg, Biophys. J. **76**, 580 (1999).
52. M. Danilchik, E.E. Brown, K. Riegert, Development **133**, 4517 (2006).
53. R. Kuroda, B. Endo, M. Abe, M. Shimizu, Nature **462**, 08597 (2009).
54. C. Pohl, Z. Bao, Dev. Cell **19**, 402 (2010).
55. Y. Wu, Basarab G. Hosu, Howard C. Berg, Proc. Natl. Acad. Sci. U.S.A. **108**, 4147 (2011).
56. M. Strempel, S. Fürthauer, S.W. Grill, F. Jülicher, arXiv:1112.3492 (2011).